Dalton Transactions

PAPER

View Article Online
View Journal | View Issue

Cite this: *Dalton Trans.*, 2014, **43**, 16640

Niobium(v) and tantalum(v) halide chalcogenoether complexes – towards single source CVD precursors for ME_2 thin films†

Sophie L. Benjamin, Yao-Pang Chang, Chitra Gurnani,‡ Andrew L. Hector, Michelle Huggon, William Levason and Gillian Reid*

A series of pentavalent niobium and tantalum halide complexes with thio-, seleno- and telluro-ether ligands, $[MCl_5(E^nBu_2)]$ (M = Nb, Ta; E = S, Se, Te), $[TaX_5(TeMe_2)]$ (X = Cl, Br, F) and the dinuclear $[(MCl_5)_2\{o\text{-}C_6H_4(CH_2SEt)_2\}]$ (M = Nb, Ta), has been prepared and characterised by IR, ^1H, $^{13}C\{^1H\}$, ^{77}Se, ^{93}Nb and ^{125}Te NMR spectroscopy, as appropriate, and microanalyses. Confirmation of the tantalum(v)–telluroether coordination follows from the crystal structure of $[TaCl_5(TeMe_2)]$, which represents the highest oxidation state transition metal complex with telluroether coordination structurally authenticated. The Ta(v) mono-telluroether complexes are much more stable than the Nb(v) analogues. In the presence of $TaCl_5$ the ditelluroether, $CH_2(CH_2Te^tBu)_2$, is decomposed; one of the products is the dealkylated $[^tBuTe(CH_2)_3Te]$-$[TaCl_6]$, whose structure was determined crystallographically. Crystal structures of $[(MCl_5)_2\{o\text{-}C_6H_4(CH_2SEt)_2\}]$ (M = Nb, Ta) show ligand-bridged species. The complexes bearing β-hydrogen atoms on the terminal alkyl substituents have also been investigated as single source reagents for the deposition of ME_2 thin films *via* low pressure chemical vapour deposition. While the tantalum complexes proved to be unsuitable, the $[NbCl_5(S^nBu_2)]$ and $[NbCl_5(Se^nBu_2)]$ deposit NbS_2 and $NbSe_2$ as hexagonal platelets onto SiO_2 substrates at 750 °C and 650 °C, respectively. Grazing incidence and in-plane X-ray diffraction confirm both materials adopt the 3R-polytype (*R3mh*), and the sulfide shows preferred orientation with the crystallites aligned predominantly with the *c* axis perpendicular to the substrate. Scanning electron microscopy and Raman spectra are consistent with the X-ray data.

Received 3rd September 2014,
Accepted 16th September 2014

DOI: 10.1039/c4dt02694b

www.rsc.org/dalton

Introduction

Interest in methods for growing thin films of the layered early transition metal chalcogenides, ME_2 (E = S, Se, Te) has increased recently due to their structural relationship as inorganic analogues of graphene, but with the benefits of higher stability and tuneability of the inorganic materials compared with graphene. A wide range of materials and functional properties are accessible by varying M and E.[1] Controlling the dimensionality of these materials is of particular interest since it allows the anisotropy of the material properties to be maximized. Hence, 2D thin films of VSe_2, $NbSe_2$ and $MoSe_2$ are highly promising candidates for use in a variety of applications such as spintronics, energy storage, electrocatalysis, optoelectronics materials, environmental sensors and magnetic materials.[2–7] Despite the attractions of these binary materials and their exciting applications, reliable methods for their deposition as thin films are still very limited, especially for E = Se and Te. Exfoliation from bulk samples has been employed recently to access ultrathin 2D films, including for VSe_2, TaE_2 (E = S, Se) and WSe_2.[8,9] Chemical vapour deposition (CVD) is a versatile, scalable and low-cost deposition method that is used widely in commercial processes for thin film coatings.[10] Several groups, including us, have investigated its application for the growth of binary chalcogenide materials with early transition metals such as Ti, Nb and V using single source or dual source routes.[11–13] Typically for sulfides, either thiolate complexes have been employed as single source reagents or a volatile metal source has been used with excess thiol in a dual source approach. With regards to the heavier chalcogenides, some success has been achieved with selenolate complexes, *e.g.* $[(\eta^5\text{-}C_5H_5)_2M(Se^tBu)_2]$ for ME_2 (M = Ti, Zr, Hf),[14] and with metal halide complexes of the neutral selenoether ligands, which form more easily handled single source

School of Chemistry, University of Southampton, Southampton SO17 1BJ, UK. E-mail: G.Reid@soton.ac.uk

†Electronic supplementary information (ESI) available: Crystal structure of $[(NbCl_5)_2\{o\text{-}C_6H_4(CH_2SEt)_2\}]$. CCDC 1022738–1022741. For ESI and crystallographic data in CIF or other electronic format see DOI: 10.1039/c4dt02694b

‡Present address: Division of Chemistry and Biological Chemistry, Nanyang Technological University, Singapore.

precursors.[11,12a,13a] However, outside of Group 4, single source CVD reagents for controlled growth of early transition metal chalcogenides are rare. Examples of telluroether complexes with these hard, strongly polarised, high oxidation state metals are extremely unusual,[15] and none have been tested as single source precursors in CVD.

With regards to the Group 5 (Nb, Ta) binary chalcogenide materials, a small number of reports have used niobium thiolate complexes for CVD of NbS_2,[12b,c] while for $NbSe_2$, the only CVD-based route uses a dual source approach from $NbCl_5$ and excess Se^nBu_2.[12a]

Here we report the synthesis and spectroscopic properties of the distorted octahedral M(v) complexes $[MCl_5(E^nBu_2)]$ (M = Nb, Ta; E = S, Se, Te), $[TaX_5(TeMe_2)]$ (X = Cl, Br, F) and the dinuclear $[(MCl_5)_2\{o\text{-}C_6H_4(CH_2SEt)_2\}]$ (M = Nb, Ta), including the crystal structures of $[TaCl_5(TeMe_2)]$ and $[(MCl_5)_2\text{-}\{o\text{-}C_6H_4(CH_2SEt)_2\}]$. We also report investigations into their application as single source reagents for the deposition of the layered binary chalcogenides, ME_2, *via* low pressure CVD. Several NbX_5 and TaX_5 chalcogenoether complexes have been reported previously,[15,16] however, in the present work ^{n}Bu, Et and *o*-xylyl organic groups were incorporated into the ligands specifically in an attempt to promote a low energy elimination pathway during the CVD process.[11–13,17]

Results and discussion

The complexes $[MCl_5(E^nBu_2)]$ (E = S, Se, Te), $[TaX_5(TeMe_2)]$ (X = Cl, Br) and the dinuclear $[(MCl_5)_2\{o\text{-}C_6H_4(CH_2SEt)_2\}]$ (M = Nb, Ta) were prepared and isolated in good yield as orange-red products by direct reaction of MX_5 with the ligand in anhydrous CH_2Cl_2 at ambient temperature, except for the telluroether reactions which were performed at 0 °C (Scheme 1). The complexes with butyl-substituted ligands are viscous oils, whereas the complexes with ethyl and methyl substituted ligands are powdered solids. As expected for complexes of niobium(v) and tantalum(v) with soft donor ligands, the isolated compounds are very moisture sensitive, particularly in solution. However, other than the $[NbCl_5(Te^nBu_2)]$, they are stable for months when stored in a N_2 purged glove box. The choice of ligand was driven by the objective to utilise them as single source CVD reagents, hence where possible, substituents with β-hydrogen atoms were chosen to take advantage of the low energy β-hydride elimination pathway, as well as to lower the lattice energy for the material, leading to favourable volatility. Far IR spectroscopy confirms the local C_{4v} symmetry associated with the $[MCl_5(L)]$ moiety, typically showing the expected three M–Cl stretching vibrations, consistent with earlier work.[15,16] In addition to microanalytical data, ^{1}H, $^{13}C\{^1H\}$, $^{77}Se\{^1H\}$, $^{125}Te\{^1H\}$ and ^{93}Nb NMR spectroscopy are fully consistent with the stated formulations.[15]

The Nb(v) telluroether complexes are particularly unstable, changing colour over a few hours at room temperature even under N_2, possibly through reduction of the metal by internal redox chemistry involving the telluroether. In contrast, the Ta(v) complexes with the mono-telluroether ligands form in excellent yield, and are readily handled under N_2 and may be stored for several months in a freezer (−18 °C). This probably reflects the increased stability of the +5 oxidation state for Ta over Nb, so that the Ta complexes are less susceptible to reduction by the telluroether. It is notable that the +5 oxidation state present in the tantalum telluroether complexes represents the highest known for any telluroether complex. Further, the $[TaCl_5(TeMe_2)]$ that we report here (*vide infra*) is the first crystallographically characterised telluroether complex of any metal ion from Groups 1 to 5 of the periodic table.[18] In view of the unexpected stability of the $[TaX_5(TeR_2)]$ (X = Cl, Br) complexes reported here, and our recent work exploring TaF_5 complexes with soft donor ligands such as phosphines[19] or thio- and selenoethers,[16] we have also investigated reaction of TaF_5 and $TeMe_2$ in a 1 : 1 molar ratio in CH_2Cl_2 at 0 °C. This initially produced a light yellow solution, and following filtration to remove minor insoluble material, the solvent was removed *in vacuo* to give a light yellow solid. This product is very unstable and darkens over a few hours even when stored as a solid under a dry N_2 atmosphere, hindering its full characterisation. This is likely to be a result of the weak binding of the soft telluroether to the very hard TaF_5 moiety. Spectroscopic data were therefore obtained from freshly prepared samples. The IR spectrum (Nujol) shows peaks at 641sh, 618s and 607sh cm^{-1} assigned to Ta–F stretching modes, consistent with the C_{4v} symmetry ($2a_1 + e$) expected for $[TaF_5(TeMe_2)]$. The ^{1}H NMR spectrum of a freshly prepared solution in CD_2Cl_2 shows a singlet at δ = 2.49 assigned to the neutral pentafluoro complex, $[TaF_5(TeMe_2)]$. A second, much weaker singlet at 2.57 ppm is due to Me_2TeF_2,[20] formed by fluorination of the telluroether by TaF_5. A weak, but sharp, singlet in

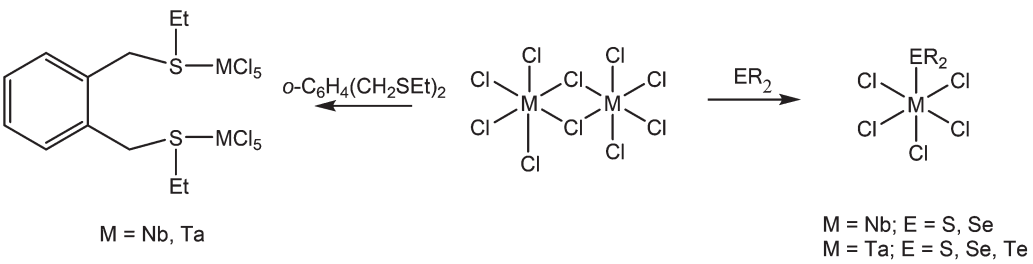

Scheme 1

the $^{19}F\{^{1}H\}$ NMR spectrum at −132.0 ppm is also due to Me_2TeF_2;[20] this is accompanied by a much more intense, broad resonance at *ca.* 73 ppm. Cooling this solution to −90 °C leads to the broad resonance shifting to 41.2 ppm and sharpening significantly. This is similar to the behaviour observed for $[TaF_5(SeMe_2)]$[16] and is attributed to the presence of the rather unstable complex $[TaF_5(TeMe_2)]$, which is extensively dissociated at room temperature. At −90 °C the low temperature limiting spectrum has not yet been reached, hence distinct resonances for the equatorial and axial Fs are not observed. Further $^{19}F\{^{1}H\}$ NMR resonances at 117.6, 71.5 and −82 ppm (in a 1 : 8 : 2 ratio) grew in over *ca.* 30 minutes, and are attributed to $[Ta_2F_{11}]^-$.[21] The ^{125}Te NMR resonance for $[TaF_5(Me_2Te)]$ was not observed, most likely due to the instability of the compound over the long accumulation time.

Confirmation of the Ta(v)–telluroether coordination follows from a single crystal X-ray structure determination of $[TaCl_5(TeMe_2)]$. The structure shows (Fig. 1) the expected distorted octahedral coordination at Ta(v), with *d*(Ta–Te) = 2.964(3) Å, and *d*(Ta–Cl) lying in the range 2.290(9) to 2.306(6) Å. The Ta–Cl *trans* to $TeMe_2$ lies at the lower end of the range, but is not significantly different from Ta–Cl *trans* to Cl. While there are no other tantalum(v)–telluroether species with which to compare the Ta–Te bond distance, the isomorphous $[TaCl_5(SeMe_2)]$ shows *d*(Ta–Se) = 2.7992(8) Å.[16]

Attempts to coordinate $TaCl_5$ to the ditelluroether, $CH_2(CH_2Te^tBu)_2$, led instead to significant Te–C bond scission and multiple products (based upon NMR spectroscopic data) – Scheme 2. One of these formed small orange crystals by cooling a CH_2Cl_2 solution in the freezer for several days. A structure determination was therefore attempted. The diffraction data were weak, and the C atoms determined less accurately, however the study was sufficient to establish this product as a $[TaCl_6]^-$ salt of the cationic cyclic organotellurium species $[^tBuTe(CH_2)_3Te]^+$ shown in Fig. 2 below. It is likely that this cation is formed by elimination of a ^{t}Bu group, followed by nucleophilic attack of the anionic Te terminus on the other Te group, forming the Te–Te bond. Similar reactivity of other telluroethers has been observed in the presence of other strongly Lewis acidic metal halides, including AlX_3.[22]

Structure determinations were also undertaken for $[(MCl_5)_2\{o\text{-}C_6H_4(CH_2SEt)_2\}]$ (M = Nb and Ta) which are isostructural, both containing six-coordinate M(v) with the ligand bridging the two MCl_5 units. The Ta complex is shown in Fig. 3 and the Nb analogue is presented in the ESI.† The M–Cl and M–S bond distances are comparable to other thioether complexes of these ions.[15,16]

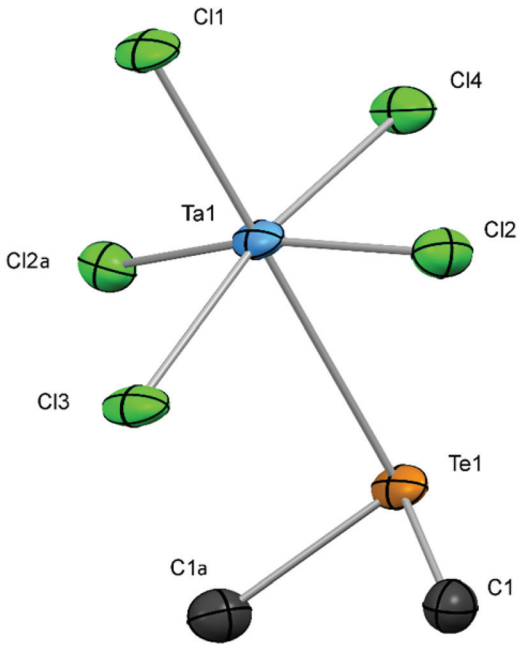

Fig. 1 View of the structure of $[TaCl_5(TeMe_2)]$ with numbering scheme adopted. Ellipsoids are drawn at the 50% probability level and H atoms are omitted for clarity. Selected bond lengths (Å) and angles (°): Ta1–Cl1 = 2.290(9), Ta1–Cl2 = 2.306(6), Ta1–Cl3 = 2.298(9), Ta1–Cl4 = 2.303(10), Ta1–Te1 = 2.964(3), Cl1–Ta1–Te1 = 179.1(2). Symmetry operation a = *–x*, *y*, *z*.

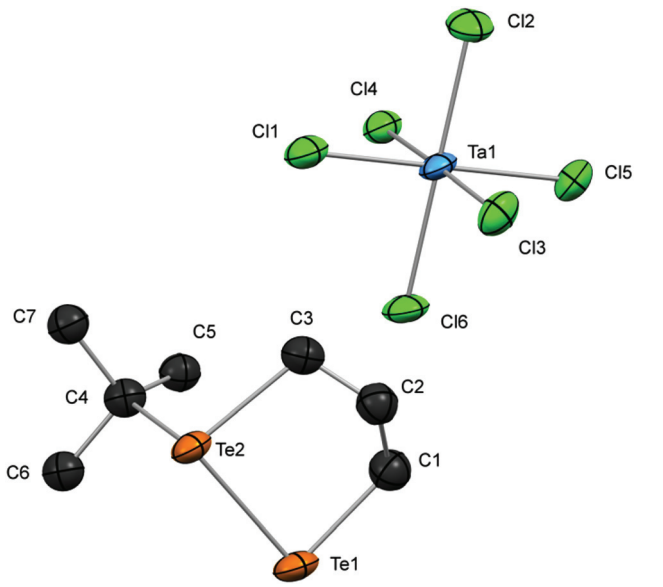

Fig. 2 View of the structure of $[^tBuTe(CH_2)_3Te][TaCl_6]$ with ellipsoids shown at the 50% probability level. Note that the data quality is poor, hence structural comparisons should be treated with caution.

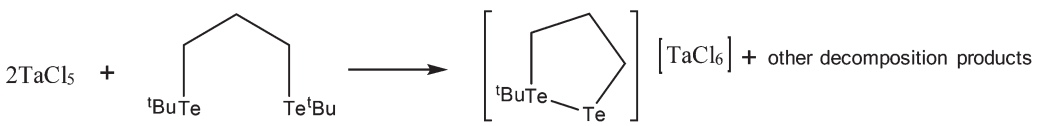

Scheme 2

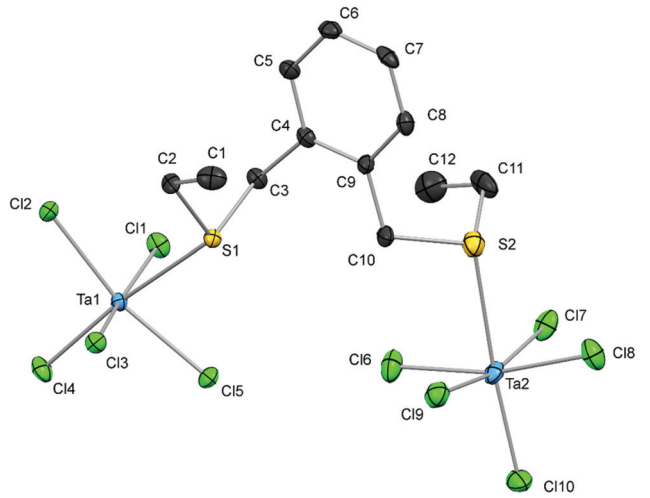

Fig. 3 View of the structure of $[(TaCl_5)_2\{o\text{-}C_6H_4(CH_2SEt)_2\}]$ with numbering scheme adopted. Ellipsoids are shown at the 50% probability level and H atoms are omitted for clarity. Selected bond lengths (Å) and angles (°): Ta1–Cl1 = 2.3019(16), Ta1–Cl2 = 2.3102(16), Ta1–Cl3 = 2.3473(15), Ta1–Cl4 = 2.2726(16), Ta1–Cl5 = 2.3341(17), Ta1–S1 = 2.6713(15), Ta2–Cl6 = 2.3258(18), Ta2–Cl7 = 2.3258(19), Ta2–Cl8 = 2.3341(18), Ta2–Cl9 = 2.3219(19), Ta2–Cl10 = 2.2607(18), Ta2–S2 = 2.7081(19), S1–Ta1–Cl4 = 170.88(5), S2–Ta2–Cl10 = 174.81(7).

CVD experiments

The complexes $[MCl_5(E^nBu_2)]$ and $[(MCl_5)_2\{o\text{-}C_6H_4(CH_2SEt)_2\}]$ (M = Nb, Ta) were all tested as potential single source CVD precursors at a range of temperatures around 600–750 °C (at a pressure *ca.* 0.05 mmHg). No significant deposition was observed at lower temperature. In general, none of the Ta reagents showed significant deposition (except for $[TaCl_5(Te^nBu_2)]$ which deposited some crystalline tellurium). However, while the dinuclear Nb(v) species appeared to be insufficiently volatile to give significant deposition, LPCVD experiments using both $[NbCl_5(S^nBu_2)]$ (T *ca.* 750 °C) and $[NbCl_5(Se^nBu_2)]$ (T *ca.* 650 °C) led to formation of reflective dark brown/black films onto the SiO_2 substrates. The thickest deposits were identified towards the centre of the hot zone and these were therefore selected for further characterisation.

The films obtained from $[NbCl_5(S^nBu_2)]$ show diffraction patterns consistent with NbS_2; the best fit being for NbS_2 in space group *R3mh* (3R-type NbS_2) (Fig. 4).[23] In some early samples minor peaks associated with niobium oxide (Nb_2O_5) were observed, however, these did not increase in intensity upon prolonged exposure (for several months) of the deposits to the atmosphere, and could be eliminated by rigorous drying of the CVD equipment and using high purity precursors. Hence it seems likely that this was a result of trace hydrolysis of the precursor. The diffraction pattern is similar to that identified by Winter and co-workers[24] using $[NbCl_4(^iPrSS^iPr)][NbCl_6]$ as a single source precursor for LPCVD of 3R-NbS_2, also with some Nb_2O_5 impurity. Lattice parameters determined by Rietveld refinement of the grazing incidence XRD pattern are: a = 3.3343(14) and c = 17.820(11) Å (R_{wp} = 5.3%, R_p = 3.5%,

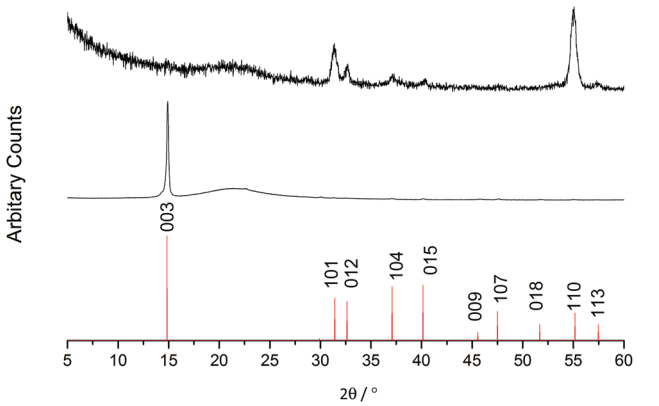

Fig. 4 In plane XRD (top), grazing incidence (incidence angle = 1°) XRD (middle) from the NbS_2 thin film deposited by LPCVD using $[NbCl_5(S^nBu_2)]$ at 750 °C; stick diagram of the XRD of bulk NbS_2 from ref. 23 (bottom). The broad feature at $2\theta \sim 22°$ is from the SiO_2 substrate.

see ESI†). These are close to literature values for bulk NbS_2 of a = 3.3303(3), c = 17.918(2) Å.[23]

Notably comparison of the grazing incidence and the in-plane XRD patterns (Fig. 4) shows considerable intensity variations for several of the diffraction peaks, consistent with preferred orientation. Specifically, the 003 reflection that is strongest in the grazing incidence XRD pattern is almost completely suppressed in the in-plane XRD pattern, while the 101, 012 and 110 reflections are highly suppressed in the grazing incidence XRD, but dominate the in-plane XRD pattern. A symmetric θ–2θ scan resulted in a very weak pattern due to the thinness of the film studied, but the combination of the grazing incidence and in-plane patterns strongly suggests crystallites are largely aligned with the <001> axis at the film surface normal such that the a and b crystallographic directions are parallel with the surface.

The Raman spectrum recorded from the deposited film is also consistent with the 3R-NbS_2 polytype (ESI†).[25] Scanning electron microscopy (SEM) images (Fig. 5) reveal that the NbS_2 films have a regular morphology formed of microcrystalline platelets mostly aligned with the *ab* plane parallel to the sub-

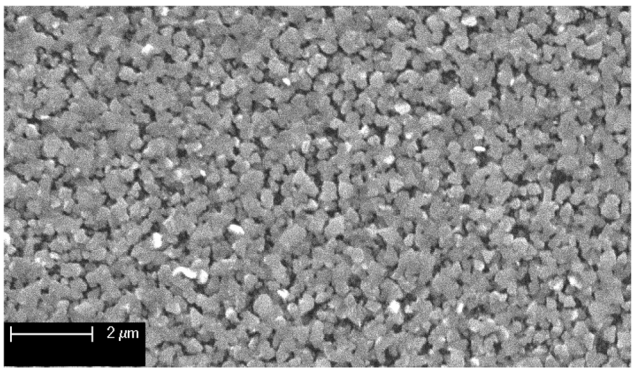

Fig. 5 SEM image of one of the NbS_2 films deposited by LPCVD from $[NbCl_5(S^nBu_2)]$ at 750 °C.

strate, as suggested by the XRD data. EDX data measured at an accelerating voltage of 5 kV to minimise break-through to the substrate still show significant Si and O in addition to peaks due to Nb and S, indicating that the films are thin; importantly, however, there is no evidence for any residual Cl in the films. Accurate quantification of the Nb : S ratio by EDX is hampered by overlap of the Nb L_α and S K_α peaks.

Films obtained using the $[NbCl_5(Se^nBu_2)]$ precursor appear shiny and dark brown/black. Grazing incidence XRD data on our films were consistent with $NbSe_2$ (space group *R*3*mh*; 3R-$NbSe_2$, Fig. 6).[26] Again, some samples showed small amounts of Nb_2O_5 impurity,[27] which could be eliminated by careful exclusion of trace moisture from the CVD rig prior to introduction of the $[NbCl_5(Se^nBu_2)]$. A previous study by Parkin and co-workers[12a] using dual source APCVD from $NbCl_5$ and excess Se^tBu_2 found dark-green or dark-purple films of the $2H_a$-$NbSe_2$ phase. The 3R phase observed here differs from the 2H phase only in the stacking sequence of the layers of edge-linked $NbSe_6$ trigonal prisms, the 2H phase has a 2-layer stacking sequence and the 3R phase has a 3-layer sequence. Rietveld refinement of the grazing incidence XRD data (ESI†) gave lattice parameters a = 3.4469(9), c = 18.940(14) Å (R_{wp} = 6.4%, R_p = 4.5%), which compare with literature values of a = 3.45(1), c = 18.880(40) Å.[26] While significant enhancement of the 003 reflection is again observed in the grazing incidence XRD and the 101 and 110 are clearly enhanced in the in-plane pattern, suggesting the same type of <001> preferred orientation, this is less pronounced than for the NbS_2 above.

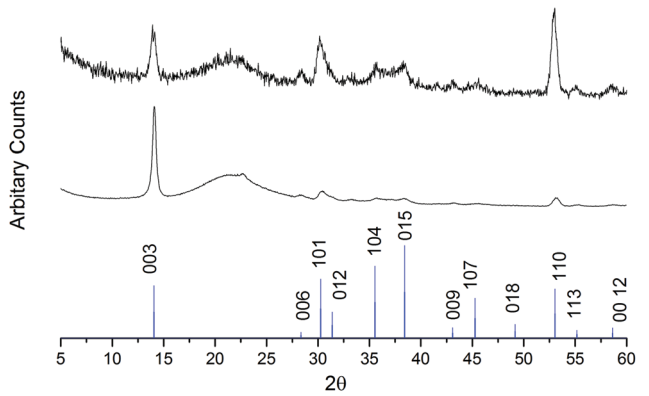

Fig. 6 In plane XRD (top), grazing incidence (incidence angle = 1°) XRD (middle) from the $NbSe_2$ thin film deposited by LPCVD using $[NbCl_5(Se^nBu_2)]$ at 650 °C. (Blue lines represent the literature pattern for bulk $NbSe_2$ taken from ref. 26.) The broad feature at $2\theta \sim 23°$ is due to the SiO_2 substrate, while the minor peaks at 2θ = 22.57 and 36.74 correspond to Nb_2O_5.[27]

Raman spectra recorded for the films deposited at 600 and 650 °C (Fig. 7) are consistent with $NbSe_2$, showing a broad peak at ~189 cm^{-1}, which has been assigned to a lattice distortion, and a stronger, sharper peak at 228 cm^{-1} with a shoulder at *ca.* 237 cm^{-1} assigned to the A_{1g} active phonon and the E_{2g} phonon mode, respectively.[28] Measurements taken at several locations on the sample showed no significant variation.

SEM images (Fig. 8) show that the $NbSe_2$ thin films are formed of hexagonal plate-like microcrystals growing out from and covering the surface of the substrate. The partial orientation identified in the XRD measurements is not as obvious here, although the enhancement of the <001> direction can be understood in terms of the observation that in general the plates do not appear to be growing perpendicular to the surface.

EDX data show the Nb : Se ratio is *ca.* 1 : 1.7 (22.40% : 38.35%), and like the sulfide films, there is no evidence for any Cl impurity, despite the Cl^- ligands present in the precursor compounds, although significant substrate peaks are seen. WDX data were also recorded for this $NbSe_2$ thin film, giving an Nb : Se ratio = 1 : 1.9, however, accurate quantification of the carbon content was not possible due to the occurrence of other Nb emission peaks at similar energy to the C peak.

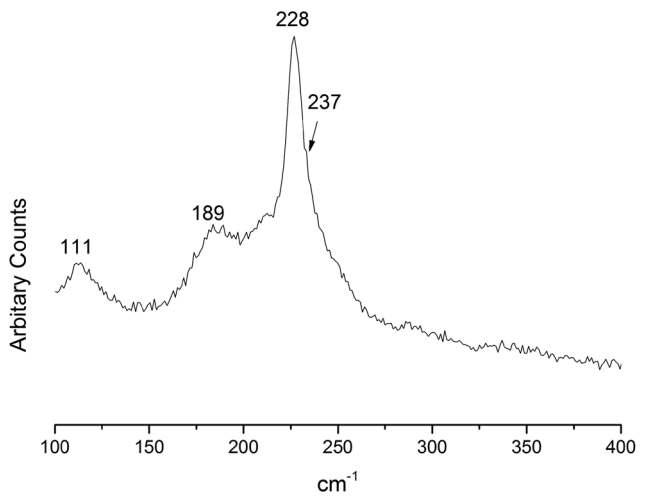

Fig. 7 Raman spectrum of the $NbSe_2$ thin film deposited by LPCVD from $[NbCl_5(Se^nBu_2)]$ at 650 °C.

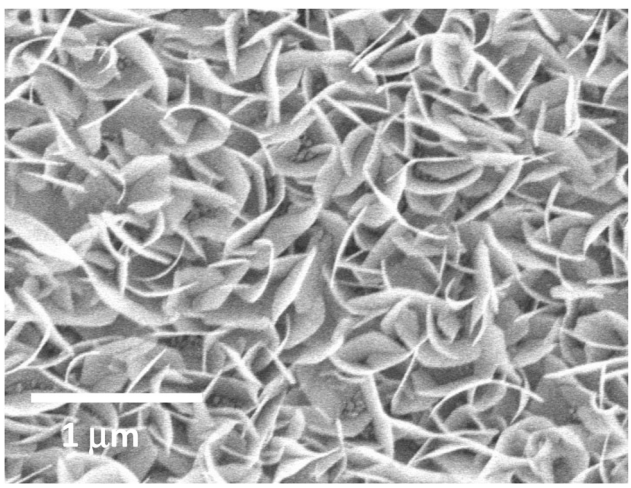

Fig. 8 SEM image of one of the $NbSe_2$ thin films deposited by LPCVD on SiO_2 at 600 °C.

Conclusions

A selected set of Nb(v) and Ta(v) complexes with chalcogenoether coordination has been prepared and the Et and ^{n}Bu substituted derivatives have been evaluated as possible single source CVD candidates for ME_2 thin films. Successful growth of NbS_2 and $NbSe_2$ thin films has been demonstrated using the $[NbCl_5(E^{n}Bu_2)]$ (E = S or Se) systems; this was rather unexpected based upon both the M : E ratio in the precursor (1 : 1) *vs.* the metal dichalcogenide phase (1 : 2), and the utilisation of the +5 oxidation state in the precursor *vs.* +4 in the ME_2. NbS_2 exhibits strong <001> preferred orientation in these thin films, whereas $NbSe_2$ exhibits enhancement of the same peaks in the XRD pattern, but to a lesser degree. The instability of the niobium(v) telluroether complexes eliminated the possibility of testing these as reagents in LPCVD.

The first detailed characterisation of Ta(v) telluroether complexes are described, including $[TaCl_5(TeMe_2)]$, which is the first crystallographically authenticated early transition metal halide telluroether complex. The tantalum(v) chalcogenoether complexes did not produce TaE_2 *via* LPVCD. There are several possible reasons for this, including the higher molecular weights associated with the Ta complexes, and hence their lower volatilities, such that the difference between the evaporation temperature and the deposition temperature is too small for an effective CVD reagent. Further work investigating alternative precursors and deposition methods will help to elucidate the key factors involved.

Experimental

Infrared spectra were recorded as Nujol mulls or thin films between CsI plates using a Perkin Elmer Spectrum 100 over the range 4000–200 cm^{-1}. ^{1}H and ^{13}C{^{1}H} NMR spectra were recorded from CD_2Cl_2 or $CDCl_3$ solutions using a Bruker DPX400 spectrometer. ^{77}Se{^{1}H}, ^{125}Te{^{1}H} and ^{93}Nb NMR spectra were recorded using a Bruker DPX400 spectrometer and are referenced to external neat $SeMe_2$ or $TeMe_2$ and $[Et_4N][NbCl_6]$ in MeCN (δ = 0), respectively. Microanalyses on new complexes were undertaken by London Metropolitan University or Medac Ltd. Preparations used standard Schlenk and glove box techniques under a N_2 atmosphere with rigorous exclusion of moisture. Solvents were dried by distillation from CaH_2 (CH_2Cl_2 or CH_3CN) or Na/benzophenone ketyl (diethyl ether). Anhydrous $NbCl_5$ and $TaCl_5$ were obtained from Aldrich and used as received. The ligands ER_2,[29] *o*-$C_6H_4(CH_2SEt)_2$,[30] $CH_2(CH_2Te^{t}Bu)_2$ [17b] and the complex $[NbCl_5(SEt_2)]$[15a] were made by literature methods or slight modifications thereof.

Preparations

$[NbCl_5(S^{n}Bu_2)]$. $NbCl_5$ (0.41 g, 1.5 mmol) was suspended in anhydrous CH_2Cl_2 (10 mL) at room temperature, and a solution of $S^{n}Bu_2$ (0.22 g, 1.5 mmol) in CH_2Cl_2 (2 mL) added with stirring. The colour changed to light orange immediately, and the solution was stirred for *ca.* 30 min. The volatiles were removed *in vacuo*, leaving an orange oil. Yield: 0.43 g, 69%. Required for $C_8H_{18}Cl_5NbS$: C, 23.07; H, 4.36%. Found: C, 23.05; H, 4.32%. ^{1}H NMR ($CDCl_3$, 298 K): δ = 0.98 (t, [3H], CH_3), 1.50 (m, [2H], CH_2), 1.79 (m, [2H], CH_2), 3.10 (t, [2H], SCH_2). ^{13}C{^{1}H} NMR ($CDCl_3$, 298 K): δ = 13.52 (CH_3), 21.86 (CH_2), 30.43 (CH_2), 39.92 (SCH_2). ^{93}Nb NMR (CD_2Cl_2, 298 K): δ = 97. IR (Nujol, cm^{-1}): 363 sh, 371 s, 394 sh (Nb–Cl).

$[NbCl_5(Se^{n}Bu_2)]$. $NbCl_5$ (0.41 g, 1.5 mmol) was suspended in anhydrous CH_2Cl_2 (10 mL) at room temperature, and a solution of $Se^{n}Bu_2$ (0.29 g, 1.5 mmol) in CH_2Cl_2 (2 mL) added with stirring. The colour changed to red-orange immediately, and the solution was stirred for *ca.* 1 hour. The volatiles were removed *in vacuo*, leaving dark red oil. Yield: 1.10 g, 79%. Required for $C_8H_{18}Cl_5NbSe$: C, 20.72; H, 3.92%. Found: C, 21.06; H, 4.33%. ^{1}H NMR ($CDCl_3$, 298 K): δ = 0.98 (t, [3H], CH_3), 1.50 (m, [2H], CH_2), 1.83 (m, [2H], CH_2), 3.14 (br, [2H], $SeCH_2$). ^{13}C{^{1}H} NMR ($CDCl_3$, 298 K): δ = 13.49 (CH_3), 22.83 (CH_2), 31.05 (CH_2), 36.62 (br, $SeCH_2$). ^{77}Se{^{1}H} NMR ($CDCl_3$, 298 K): δ = 273.6. ^{93}Nb NMR ($CDCl_3$, 298 K): δ = 123. IR (Nujol, cm^{-1}): 340 m, 372 s, 394 s (Nb–Cl).

Attempted preparation of $[NbCl_5(Te^{n}Bu_2)]$. $NbCl_5$ (0.27 g, 1.0 mmol) was suspended in anhydrous CH_2Cl_2 (10 mL) at 0 °C (ice bath), and a solution of $Te^{n}Bu_2$ (0.24 g, 1.0 mmol) in CH_2Cl_2 (4 mL) added with stirring. The colour changed to purple-blue immediately, and after *ca.* 10 min. the volatiles were removed and the remaining blue oil was dried *in vacuo*. The compound appeared to change colour over a few hours, hence spectroscopic data were obtained from a freshly prepared sample, but we were unable to obtain either microanalytical data (outsourced) or ^{125}Te{^{1}H} NMR data due sample degradation over the long spectral acquisition time. ^{1}H NMR ($CDCl_3$, 298 K): δ = 0.98 (t, [6H], CH_3), 1.48 (m, [4H], CH_2), 1.87 (m, [4H], CH_2), 3.13 (s, [4H], CH_2). ^{93}Nb NMR ($CDCl_3$, 298 K): δ = 169. IR (Nujol, cm^{-1}): 340 m, 367 s, 388 sh (Nb–Cl).

$[(NbCl_5)_2\{o\text{-}C_6H_4(CH_2SEt)_2\}]$. $NbCl_5$ (0.54 g, 2.0 mmol) was suspended in anhydrous CH_2Cl_2 (20 mL) at room temperature, and a solution of *o*-$C_6H_4(CH_2SEt)_2$ (0.23 g, 1.0 mmol) in CH_2Cl_2 (20 mL) was added with stirring. The colour changed to light orange, and the reaction mixture was stirred for 1 h, then concentrated *in vacuo* to *ca.* 10 mL. Some orange powder formed and was removed by filtration and discarded. The orange filtrate was then placed in the freezer (−18 °C) for a few days, furnishing orange crystals suitable for crystallographic analysis. Yield: 0.21 g, 27%. Required for $C_{12}H_{18}Cl_{10}Nb_2S_2$: C, 18.79; H, 2.37%. Found: C, 18.80; H, 2.58%. ^{1}H NMR ($CDCl_3$, 298 K): δ = 1.26 (br s, [6H], CH_3), 3.06 (br, [4H], CH_2CH_3), 4.41 (s, [4H], ar-CH_2), 7.41 (m, [4H], aromatic-CH). ^{93}Nb NMR ($CDCl_3$, 298 K): δ = 94. IR (Nujol, cm^{-1}): 345 m, 373 s, 397 sh (Nb–Cl).

$[TaCl_5(SEt_2)]$. $TaCl_5$ (0.36 g, 1.0 mmol) was suspended in CH_2Cl_2 at room temperature under N_2. SEt_2 (0.11 mL, 1.0 mmol) was added slowly, causing an immediate colour change to yellow. The reaction was stirred for 3 hours and then filtered. The filtrate was concentrated *in vacuo* to remove all volatiles,

leaving a yellow/orange oil. Yield: 0.31 g, 69%. Required for $C_4H_{10}Cl_5STa$: C, 10.72; H, 2.25%. Found: C, 10.56; H, 2.16%. ^{1}H NMR ($CDCl_3$): δ = 1.49 (t, [6H], CH_3), 3.27 (q, [4H], SCH_2). IR (thin film, cm^{-1}): 317 sh, 335 s, 389 m (Ta–Cl).

[$(TaCl_5)_2${*o*-$C_6H_4(CH_2SEt)_2$}]. $TaCl_5$ (0.36 g, 1.0 mmol) was suspended in CH_2Cl_2 (10 mL) at room temperature under N_2. *o*-$C_6H_4(CH_2SEt)_2$ (0.11 g, 0.5 mmol) in CH_2Cl_2 (5 mL) was added, causing a rapid colour change to yellow. The solution was concentrated *in vacuo* to around 5 mL, hexane (5 mL) was added, causing precipitation of a yellow solid, which was collected by filtration. The filtrate was placed in the freezer (−18 °C) where single crystals grew over a few days. Yield: 0.28 g, 59%. Required for $C_{12}H_{18}Cl_{10}S_2Ta_2$: C, 15.29; H, 1.92%. Found: C, 15.43; H, 1.79%. ^{1}H NMR ($CDCl_3$, 298 K): δ = 1.25 (t, [6H], CH_3), 3.2 (br, [4H], SCH_2CH_3), 2.25 (br s, [4H], SCH_2), 7.43 (m, [4H], aromatic-CH). IR (Nujol, cm^{-1}): 343 s, 366 m sh, 392 m (Ta–Cl).

[$TaCl_5(S^nBu_2)$]. $TaCl_5$ (0.18 g, 0.5 mmol) was suspended in anhydrous CH_2Cl_2 (5 mL) at room temperature, and S^nBu_2 (0.09 mL, 0.5 mmol) was added with stirring. The colour changed immediately from colourless to lemon yellow. After *ca.* 10 min. the solution was filtered to remove any particulates and all volatiles were removed *in vacuo*, leaving an orange oil. Yield: 0.11 g, 45%. ^{1}H NMR ($CDCl_3$, 298 K): δ = 0.98 (t, [3H], CH_3), 1.50 (m, [2H], CH_3CH_2), 1.78 (m, [2H], CH_2), 3.22 (t, [2H], SCH_2). ^{13}C{^{1}H} NMR ($CDCl_3$, 298 K): δ = 13.50 (CH_3), 21.77 (CH_3CH_2), 30.42 (CH_2), 39.79 (br, SCH_2). IR (Nujol, cm^{-1}): 318 sh, 348 s, 393 s (Ta–Cl).

[$TaCl_5(Se^nBu_2)$]. $TaCl_5$ (0.36 g, 1.0 mmol) was suspended in CH_2Cl_2 (8 mL) at room temperature under N_2. Se^nBu_2 (0.19 g, 1 mmol) dissolved in CH_2Cl_2 (2 mL) was then added. The solution turned lemon yellow immediately and was stirred for 1 h. The solution was filtered and all volatiles were then removed *in vacuo* to leave a yellow oil. Yield: 0.34 g, 61%. Required for $C_8H_{18}Cl_5SeTa$: C, 17.43; H, 3.29%. Found: C, 17.08; H, 3.48%. ^{1}H NMR ($CDCl_3$, 298 K): δ = 0.98 (t, [6H], CH_3), 1.50 (m, [4H], CH_2), 1.82 (m, [4H], CH_2), 3.26 (br, [4H], $SeCH_2$). ^{13}C{^{1}H} NMR ($CDCl_3$, 298 K): δ = 13.47 (CH_3), 22.76 (CH_2), 31.05 (CH_2), 36.76 ($SeCH_2$). ^{77}Se{^{1}H} NMR (CH_2Cl_2, 298 K): δ = 225.4. IR (thin film, cm^{-1}): 321 sh, 339 s, 387 sh (Ta–Cl).

[$TaCl_5(Te^nBu_2)$]. $TaCl_5$ (0.36 g, 1.0 mmol) was suspended in CH_2Cl_2 (7 mL) at 0 °C under N_2. Te^nBu_2 (0.24 g, 1.0 mmol) in CH_2Cl_2 (3 mL) at 0 °C was added dropwise, causing a rapid colour change to bright orange. After stirring for 2 hours, the solution was filtered to remove particulates and all volatiles were then removed *in vacuo*, leaving a bright orange/red oil. Yield: 0.40 g, 67%. Required for $C_8H_{18}Cl_5TaTe$: C, 16.01; H, 3.02%. Found: C, 16.10; H, 3.36%. ^{1}H NMR ($CDCl_3$, 298 K): δ = 0.99 (t, [6H], CH_3), 1.49 (m, [4H], CH_2), 1.84 (m, [4H], CH_2), 3.20 (br, [4H], $TeCH_2$). ^{13}C{^{1}H} NMR ($CDCl_3$, 298 K): δ = 13.38 (CH_3), 21.46 ($TeCH_2$), 24.81 (CH_2), 31.74 (CH_2). ^{125}Te{^{1}H} NMR (CH_2Cl_2, 298 K): δ = 268. IR (thin film, cm^{-1}): 317 sh, 335 s, 383 m (Ta–Cl).

[$TaCl_5(TeMe_2)$]. $TaCl_5$ (0.36 g, 1.0 mmol) was suspended in CH_2Cl_2 (7 mL) at 0 °C under N_2. $TeMe_2$ (0.16 g, 1.0 mmol) in CH_2Cl_2 (3 mL) at 0 °C was added dropwise. The solution turned bright orange immediately. After stirring for 2 h, and filtering to remove particulates, all volatiles were removed *in vacuo*, leaving a bright orange solid. Yield: 0.20 g, 39%. Required for $C_2H_6Cl_5TaTe$: C, 4.66; H, 1.17%. Found: C, 5.03; H, 1.35%. ^{1}H NMR ($CDCl_3$, 298 K): δ = 2.48 (s, CH_3). ^{13}C{^{1}H} NMR ($CDCl_3$, 298 K): δ = −1.93 (CH_3). ^{125}Te{^{1}H} NMR (CH_2Cl_2, 298 K): δ = 102. IR (Nujol, cm^{-1}): 300 sh, 338 s, 379 m (Ta–Cl). Crystals suitable for X-ray structure determination were obtained by cooling a CH_2Cl_2 solution in the freezer (−18 °C) for 2 days.

[$TaBr_5(TeMe_2)$]. Method as for [$TaCl_5(TeMe_2)$] above. Deep red powdered solid. Yield: 65%. Required for $C_2H_6Br_5TaTe$: C, 3.25; H, 0.82%. Found: C, 3.50; H, 1.16%. ^{1}H NMR (CD_2Cl_2, 298 K): δ = 2.55 (s, CH_3). ^{13}C{^{1}H} NMR (CD_2Cl_2, 298 K): δ = 1.12 (CH_3). ^{125}Te{^{1}H} NMR (CH_2Cl_2, 298 K): δ = 107. IR (Nujol, cm^{-1}): 221 m br, 230 sh (Ta–Br).

[$TaF_5(TeMe_2)$]. TaF_5 (0.28 g, 1.0 mmol) and $TeMe_2$ (0.16 g, 1.0 mmol) were weighed inside a glove box. The TaF_5 was suspended in anhydrous CH_2Cl_2 (3 mL) and the Me_2Te was mixed with anhydrous CH_2Cl_2 (2 mL); both solutions were then cooled in an ice bath. The Me_2Te solution was then added to the TaF_5 solution, causing a colour change to yellow green. After stirring for *ca.* 15 min. the colour changed to lemon. All volatiles were then removed *in vacuo* leaving a light yellow solid. IR (Nujol, cm^{-1}): 641sh, 618s, 607sh (Ta–F). ^{1}H NMR (CD_2Cl_2, 298 K): δ 2.50 (s, CH_3, major), 2.57 (s, Me_2TeF_2, minor). ^{19}F{^{1}H} NMR (CD_2Cl_2, 298 K): δ = 73 (br, [$TaF_5(TeMe_2)$], major), −132.0 (s, Me_2TeF_2, minor); (178 K): δ = 41.2 (s, [$TaF_5(TeMe_2)$], major), −132.0 (s, Me_2TeF_2, minor). ^{125}Te{^{1}H} NMR (CD_2Cl_2, 298 K): no resonances observed.

Attempted preparation of [$(TaCl_5)_2${$CH_2(CH_2Te^tBu)_2$}]. $TaCl_5$ (0.18 g, 0.5 mmol) was suspended in CH_2Cl_2 (7 mL) at 0 °C (ice bath) under N_2. $CH_2(CH_2Te^tBu)_2$ (0.11 g, 0.25 mmol) in CH_2Cl_2 (3 mL) at 0 °C was added dropwise. The solution turned dark red immediately and stirring was maintained for 15 min. The volatiles were removed *in vacuo*, leaving a dark red-orange viscous oil. ^{1}H NMR spectroscopy ($CDCl_3$) showed multiple ^{t}Bu resonances, indicative of a mixture of products suggesting decomposition. A few small, weakly diffracting crystals of [^{t}BuTe$(CH_2)_3$Te][$TaCl_6$] were obtained by cooling a CH_2Cl_2 solution of this product mixture in the freezer (−18 °C) for *ca.* one week.

X-ray experimental

Details of the crystallographic data collection and refinement parameters are given in Table 1. Crystals suitable for single crystal X-ray analysis were obtained as described. Data collections used a Rigaku AFC12 goniometer equipped with an enhanced sensitivity (HG) Saturn724+ detector mounted at the window of an FR-E+ SuperBright molybdenum (λ = 0.71073 Å) rotating anode generator with VHF Varimax optics (70 μm focus) with the crystal held at 100 K (N_2 cryostream). Structure solution and refinements were performed with SHELX(S/L)-97 [31] and were straightforward except as detailed below. H atoms bonded to C were placed in calculated positions using the default C–H distance and refined using a riding

Table 1 X-Ray crystallographic data[a]

Compound	$[TaCl_5(TeMe_2)]$	$[(TaCl_5)_2(o\text{-}C_6H_4(CH_2SEt)_2)]$	$[^tBuTe(CH_2)_3Te][TaCl_6]$
Formula	$C_2H_6Cl_5TaTe$	$C_{12}H_{18}Cl_{10}S_2Ta_2$	$C_7H_{15}Cl_6TaTe_2$
M	515.87	942.78	748.06
Crystal system	Orthorhombic	Monoclinic	Monoclinic
Space group (no.)	$Cmc2_1$ (36)	$P2_1/c$ (14)	$P2_1/c$ (14)
a/Å	8.023(5)	12.437(5)	7.433(1)
b/Å	11.998(7)	17.574(3)	9.1611(12)
c/Å	10.752(6)	11.745(2)	25.663(3)
α/°	90	90	90
β/°	90	98.859(7)	90.217(6)
γ/°	90	90	90
U/Å^3	1034.9(11)	2536.3(11)	1747.5(4)
Z	4	4	4
μ(Mo-K$_\alpha$)/mm^{-1}	14.601	9.840	10.455
Total number reflns	1827	12 901	11 709
Unique reflns	929	5770	3163
R_{int}	0.078	0.026	0.206
No. of params, restraints	49, 24	237, 0	147, 81
R_1, wR_2 $[I > 2\sigma(I)]^b$	0.063, 0.158	0.038, 0.092	0.105, 0.205
R_1, wR_2 (all data)	0.068, 0.165	0.042, 0.094	0.194, 0.244

[a] Common items: T = 100 K; wavelength (Mo-K$_\alpha$) = 0.71073 Å; θ(max) = 27.5°. [b] $R_1 = \sum||F_o|-|F_c||/\sum|F_o|$; w$R_2 = [\sum w(F_o^2-F_c^2)^2/\sum wF_o^4]^{1/2}$.

model, except for $[(TaCl_5)_2\{o\text{-}C_6H_4(CH_2SEt)_2\}]$, in which the H atom positions were calculated. The diffraction data obtained for the decomposition product, $[^tBuTe(CH_2)_3Te][TaCl_6]$, were weak and showed some evidence of twinning. Correspondingly the final structure solution is of only modest quality, with higher than normal residuals. The heavy atoms (Ta, Te and Cl) were well-defined, however the C atoms required restraints for satisfactory refinement. While the structure serves to confirm the identity of the compound, a decomposition product, comparison of geometric parameters is not warranted.

LPCVD general procedure

The single source precursor (0.02–0.10 g) was loaded into the end of silica tubes in an N_2 purged glove box. Then the silica substrates (~1 × 8 × 20 mm^3 or 0.5 × 8 × 12 mm^3) also were loaded in the tube and placed end-to-end. The tube was set in a furnace so that the substrates were in the heated zone and the precursor was *ca.* 2 cm away from the start of the heated zone. The tube was evacuated to 0.5 mm Hg, and the furnace was heated to the requisite temperature between 600 and 800 °C. The tube was then moved gradually into the furnace so that the precursor moved closer to the hot zone until it began to evaporate. The position of the sample was maintained until the all the precursor had evaporated. The tube was then cooled to room temperature and the tiles were unloaded inside a dry N_2-purged glove box, where they were stored for further characterisation. LPCVD from $[NbCl_5(S^nBu_2)]$ and $[NbCl_5(Se^nBu_2)]$ resulted in deposition of a reflective black film on tiles positioned in the hotter region of the furnace, with thinner deposits at either end.

Film characterisation

Scanning electron microscopy (SEM) was performed on samples at an accelerating voltage of 15 kV using a JEOL JSM5910 or at accelerating voltage from 5 kV to 15 KV using a Philips XL30 ESEM. Energy dispersive X-ray (EDX) data were obtained with an Oxford INCA x-act X-ray detector (JSM5910) or Thermofisher Ultradry NSS 3 (XL30). X-Ray diffraction (XRD) patterns were collected in grazing incidence mode (θ_1 = 1°) or in-plane mode (θ_1 = 0.5°, $2\theta_\chi$ scan with the detector scanning in the film plane) using a Rigaku SmartLab diffractometer (Cu-K$_\alpha$, λ = 1.5418 Å) with parallel X-ray beam and a DTex Ultra 250 1D detector. Phase matching used the PDXL2 software package[32] and diffraction patterns from ICSD.[33] Raman spectra of the deposited films were acquired with a Renishaw 2000 microscope instrument equipped with a 632.8 nm He–Ne laser and Prior XYZ stage controller. The diameter of the laser spot was 1 μm. Typically, a single 120 s acquisition was used to acquire spectra.

Acknowledgements

We thank the EPSRC for a Doctoral Prize (S.L.B.) and for provision of thin film X-ray diffraction instrument (EP/K00509X/1 and EP/K009877/1), STFC for funding (ST/L003376/1) and the Royal Society for a Newton International Fellowship (C.G.). We also thank Dr M. E. Light for assistance with X-ray data processing and Miss J. Burt and Mr R. Huang for assistance with the Raman measurements.

References

1 M. Chhowalla, H. S. Shin, G. Eda, L.-J. Li, K. P. Loh and H. Zhang, *Nat. Chem.*, 2013, **5**, 263.
2 H. Zeng, J. Dai, W. Yao, D. Xiao and X. Cui, *Nat. Nanotechnol.*, 2012, **7**, 490.
3 J. Liu and X.-W. Liu, *Adv. Mater.*, 2012, **24**, 4097.

4 Q. Xiang, J. Yu and M. Jaroniec, *J. Am. Chem. Soc.*, 2012, **134**, 6575.
5 J. Pu, Y. Yomogida, K.-K. Liu, L.-J. Li, Y. Iwasa and T. Takenobu, *Nano Lett.*, 2012, **12**, 4013.
6 K. Lee, R. Gatensby, N. McEvoy, T. Hallam and G. S. Duesberg, *Adv. Mater.*, 2013, **25**, 6699.
7 Y. Ma, Y. Dsi, M. Guo, C. Niu, Y. Zhu and B. Huang, *ACS Nano*, 2012, **6**, 1695.
8 K. Xu, P. Chen, X. Li, C. Wu, Y. Guo, J. Zhao, X. Wu and Y. Xie, *Angew. Chem., Int. Ed.*, 2013, **52**, 10477.
9 (*a*) H. Li, G. Lu, Y. Wang, Z. Yin, C. Cong, Q. He, L. Wang, F. Ding, T. Yu and H. Zhang, *Small*, 2013, **9**, 1974; (*b*) Z. Yan, C. Jiang, T. R. Pope, C. F. Tsang, J. L. Stickney, P. Goli, J. Renteria, T. T. Salguero and A. A. Balandin, *J. Appl. Phys.*, 2013, **114**, 204301.
10 A. C. Jones and M. L. Hitchman, in *Chemical Vapour Deposition: Precursors, Processes and Applications*, ed. A. C. Jones and M. L. Hitchman, The Royal Society of Chemistry, 2009.
11 (*a*) P. J. McKarns, T. S. Lewkebandara, G. P. A. Yap, L. M. Liable-Sands, A. L. Rheingold and C. H. Winter, *Inorg. Chem.*, 1998, **37**, 418; (*b*) S. D. Reid, A. L. Hector, W. Levason, G. Reid, B. J. Waller and M. Webster, *Dalton Trans.*, 2007, 4769; (*c*) S. L. Benjamin, C. H. de Groot, C. Gurnani, A. L. Hector, R. Huang, K. Ignatyev, W. Levason, S. J. Pearce, F. Thomas and G. Reid, *Chem. Mater.*, 2013, **25**, 4719; (*d*) N. D. Boscher, C. J. Carmalt and I. P. Parkin, *Chem. Vap. Deposition*, 2006, **12**, 54.
12 (*a*) N. D. Boscher, C. J. Carmalt and I. P. Parkin, *Eur. J. Inorg. Chem.*, 2006, 1255; (*b*) E. S. Peters, C. J. Carmalt, I. P. Parkin and D. A. Tocher, *Eur. J. Inorg. Chem.*, 2005, 4179; (*c*) C. J. Carmalt, E. S. Peters, I. P. Parkin, T. D. Manning and A. L. Hector, *Eur. J. Inorg. Chem.*, 2004, 4470.
13 (*a*) N. D. Boscher, C. S. Blackman, C. J. Carmalt, I. P. Parkin and A. Garcia Prieto, *Appl. Surf. Sci.*, 2007, **253**, 6041; (*b*) A. L. Hector, M. Jura, W. Levason, S. D. Reid and G. Reid, *New J. Chem.*, 2009, **33**, 641.
14 A. L. Hector, W. Levason, G. Reid, S. D. Reid and M. Webster, *Chem. Mater.*, 2008, **20**, 5100.
15 (*a*) M. Jura, W. Levason, R. Ratnani, G. Reid and M. Webster, *Dalton Trans.*, 2010, **39**, 883; (*b*) A. Merbach and J. C. Bunzil, *Helv. Chim. Acta*, 1972, **55**, 580; (*c*) R. Good and A. E. Merbach, *Helv. Chim. Acta*, 1974, **57**, 1192; (*d*) R. Good and A. E. Merbach, *Inorg. Chem.*, 1975, **14**, 1030.
16 S. L. Benjamin, A. Hyslop, W. Levason and G. Reid, *J. Fluorine Chem.*, 2012, **137**, 77.
17 (*a*) C. H. de Groot, C. Gurnani, A. L. Hector, R. Huang, M. Jura, W. Levason and G. Reid, *Chem. Mater.*, 2012, **24**, 4442; (*b*) K. George, C. H. de Groot, C. Gurnani, A. L. Hector, R. Huang, M. Jura, W. Levason and G. Reid, *Chem. Mater.*, 2013, **25**, 1829; (*c*) S. L. Benjamin, C. H. de Groot, C. Gurnani, A. L. Hector, R. Huang, E. Koukharenko, W. Levason and G. Reid, *J. Mater. Chem. A*, 2014, **2**, 4865.
18 Cambridge Structural Database accessed on the 25th July 2014. http://www.ccdc.cam.ac.uk.
19 W. Levason, M. E. Light, G. Reid and W. Zhang, *Dalton Trans.*, 2014, **43**, 9557.
20 T. Klapötke, B. Krumm, P. Mayer, H. Piotrowski, O. P. Ruscitti and A. Schiller, *Inorg. Chem.*, 2002, **41**, 1184.
21 S. Brownstein, *Inorg. Chem.*, 1973, **12**, 584.
22 K. George, M. Jura, W. Levason, M. E. Light and G. Reid, *Dalton Trans.*, 2014, **43**, 3637.
23 B. Morosin, *Acta Crystallogr., Sect. B: Struct. Crystallogr. Cryst. Chem.*, 1974, **30**, 551.
24 P. J. McKarns, M. J. Heeg and C. H. Winter, *Inorg. Chem.*, 1998, **37**, 4743.
25 W. G. McMullan and J. C. Irwin, *Solid State Commun.*, 1983, **45**, 557.
26 B. E. Brown and D. J. Beerntsen, *Acta Crystallogr.*, 1965, **18**, 31.
27 V. K. Kato and S. Tamura, *Acta Crystallogr., Sect. B: Struct. Crystallogr. Cryst. Chem.*, 1975, **31**, 673.
28 C. M. Pereira and W. Y. Liang, *J. Phys. C: Solid State Phys.*, 1985, **18**, 6075.
29 (*a*) D. J. Gulliver, E. G. Hope and W. Levason, *J. Chem. Soc., Perkin Trans. 2*, 1984, **3**, 429; (*b*) E. G. Hope, T. Kemmit and W. Levason, *Organometallics*, 1987, **6**, 206.
30 W. Levason, M. Nirwan, R. Ratnani, G. Reid, N. Tsoureas and M. Webster, *Dalton Trans.*, 2007, 439.
31 G. M. Sheldrick, *Acta Crystallogr., Sect. A: Fundam. Crystallogr.*, 2008, **64**, 112.
32 S. Grazulis, D. Chateigner, R. T. Downs, A. F. Yokochi, M. Quiros, L. Lutterotti, E. Manakova, J. Butkus, P. Moeck and A. Le Bail, *J. Appl. Crystallogr.*, 2009, **42**, 726.
33 ICSD: Inorganic Crystal Structure Database (ICSD), Fachinformationszentrum Karlsruhe (FIZ), accessed *via* the United Kingdom Chemical Database Service: D. A. Fletcher, R. F. McMeeking and D. J. Parkin, *Chem. Inf. Comput. Sci.*, 1996, **36**, 746.

